Establishment of a stem cell administration imaging method in bleomycin- induced pulmonary fibrosis mouse models

Saho Morita
Nagoya University, Graduate School of Engineering
Mayumi Iwatake (iwatake@nanobio.nagoya-u.ac.jp)
Nagoya University
Sakura Suga
Nagoya University, Graduate School of Engineering
Kazuomi Takahashi
Nagoya University Institute for Advanced Research, Nagoya University
Kazuhide Sato
Nagoya University Institute for Advanced Research, Nagoya University
Chika Miyagi-Shiohira
University of the Ryukyus
Hirofumi Noguchi
University of the Ryukyus
Yoshinobu Baba
Nagoya University, Graduate School of Engineering
Hiroshi Yukawa
Nagoya University, Graduate School of Engineering

Article

Keywords:

Posted Date: November 23rd, 2023

DOI: https://doi.org/10.21203/rs.3.rs-3569134/v1

Additional Declarations: No competing interests reported.

Abstract

Pulmonary fibrosis is a progressive disease caused by interstitial inflammation. Treatments are extremely scarce; therapeutic drugs and transplantation therapies are not widely available due to cost and a lack of donors, respectively. Recently, there has been a high interest in regenerative medicine and exponential advancements in stem cell-based therapies have occurred. However, a sensitive imaging technique for investigating the *in vivo* dynamics of transplanted stem cells has not yet been established and the mechanisms of stem cell-based therapy remain largely unexplored.

In this study, we administered adipose tissue-derived mesenchymal stem cells (ASCs) labeled with quantum dots (QDs; 8.0 nM) to a mouse model of bleomycin-induced pulmonary fibrosis in an effort to clarify the relationship between *in vivo* dynamics and therapeutic efficacy. These QD-labeled ASCs were injected into the trachea of C57BL/6 mice seven days after bleomycin administration to induce fibrosis in the lungs. The therapeutic effects and efficacy were evaluated via *in vivo/ex vivo* imaging, CT imaging, and H&E staining of lung sections.

The QD-labeled ASCs remained in the lungs longer and suppressed fibrosis. The 3D imaging results showed that the transplanted cells accumulated in the peripheral and fibrotic regions of the lungs. These results indicate that ASCs may play a significant role in the therapeutic effects of pulmonary fibrosis. Thus, QD labeling could be a suitable and sensitive imaging technique for evaluating *in vivo* kinetics in correlation with the efficacy of cell therapy.

Introduction

Idiopathic pulmonary fibrosis (IPF) is a disease in which inflammation occurs in the stroma, causing the stroma to become thick and hard and the entire lung to become fibrotic [1–4]. The cause of this progressive disease is unknown and the duration of survival from symptom onset is generally three to five years [5]. Conventional treatments include antifibrotic agents and lung transplantation; however, these are not widely used due to the lack of effective drugs and shortage of donors [6, 7]. In recent years, the expectations of regenerative medicine have increased. Stromal stem cell therapy is desirable for the treatment of pulmonary fibrosis because it is less invasive and highly effective. Despite several studies on the efficacy of stem cell therapy for pulmonary fibrosis, it has not yet been applied clinically. This is because the *in vivo* behavior of transplanted stem cells and their therapeutic effects are poorly understood, and therapeutic strategies have not been optimized. Therefore, it is extremely important to develop a technology to clarify the relationship between the *in vivo* behavior of transplanted stem cells and their therapeutic effects in order to provide stem cell therapy for IPF.

In this study, we focus on quantum dots (QDs), which are the most advanced quantum nanomaterials based on quantum nano-optics. QDs show high brightness, long-term stability, and light-resistance and are currently used in industrial applications such as 4K/8K displays and solar cells [8–10]. For application in regenerative medicine, there are established stem cell labeling and *in vivo* fluorescence imaging

technologies for transplanted stem cells using QDs with strong fluorescence in the near-infrared region (around 700–900 nm), which is highly permeable to physiological tissues (called the "biological-tissue transparency window") [11]. QDs are colloidal semiconductor nanoparticles in which the electrons are confined within a microscopic nanospace. The crystal size of these particles is less than 20 nm in diameter; at this size, the electrons are confined three-dimensionally to a limited area. QDs have excellent optical properties that are completely different from those of organic fluorochromes and fluorescent proteins, which are conventionally used for fluorescent labeling [12].

In this study, we administered adipose tissue-derived stem cells (ASCs) labeled with QDs, which have excellent fluorescence properties, to a bleomycin pulmonary fibrosis mouse model (BLM mice) in an effort to evaluate the *in vivo* behaviors and therapeutic effects of transplanted stem cells.

Results

Labeling of ASCs with QDs

First, QDs were introduced into the ASCs. In this process, octaarginine (R8), a membrane-permeable peptide, was combined with QDs. The labeling efficiency was examined using a flow cytometer with three QD concentrations: 0, 4, and 8 nM. The labeling efficiency was 97.0 ± 0.2% at 8 nM, which was the highest of the set conditions. Because the QDs used in this study had cadmium selenide in the core, potential toxicity to organisms must be carefully considered. The results of the toxicity tests showed that the QDs were not toxic up to 8 nM out of five different concentrations (0, 2, 4, 8, and 16 nM). Therefore, we used 8 nM as the concentration for QD labeling and performed *in vitro* fluorescence imaging. Because the results suggested that the QDs were introduced into the cell membrane, subsequent experiments were conducted under these conditions.

Analysis of structural changes over time using computed tomography imaging

To evaluate the therapeutic effects of ASCs in BLM mice, 800 QD-labeled ASCs were administered through the tail veins of mice 7 days after BLM mice were created. The treated and untreated BLM mice were observed over time using a small animal micro-computed tomography (CT) scanner. CT imaging showed frosted shadows and widening of the bronchi. Cross-sectional images of the lungs of untreated mice showed that the ground-glass opacity gradually became darker and wider as the days passed, whereas the ASC-treated group showed suppressed spreading of the shadows (Fig. 1A). The histograms obtained by taking cross-sectional images of the whole lungs and integrating the CT values showed that the untreated BLM mice had a higher shift in CT values with the spread of white shadows over time; this shift was suppressed in the ASC-treated group (Fig. 1B). Furthermore, lung volumes calculated from CT images of each lung section, assuming that CT values of -900 to -200 were normal, indicated that the reduction in lung volume due to fibrosis was suppressed in the ASC-treated group. The survival rate of mice was 25% (n = 12) in the untreated group and 100% in the ASC-treated group (Fig. 1C). These results

indicate that treatment with ASCs significantly suppressed the decrease in lung volume caused by fibrosis (Fig. 1B).

Evaluation of lung tissue after administration of ASCs

CT images were acquired through 3 days after the administration of ASCs to BLM mice. The images of pulmonary fibrosis showed bronchiectasis due to fibrosis and widening of the interstitial shadow due to interstitial thickening. The CT images showed that the dilated bronchi in the ASC-treated group recovered to their pre-treatment size from day 2 to day 3. (Fig. 2A). Three days after the administration of ASCs to BLM mice, bronchoalveolar lavage was performed and the surfactant protein D (SP-D) concentration in the lavage fluid was measured. Normal SP-D concentrations are around 1,100 ng/mL, but values of ASCs treated group (964.5 ng/mL) were much higher in the untreated group. This suggests that alveolar destruction occurred in the lungs. In contrast, the ASC-treated group showed normal SP-D values, indicating the repair of the destroyed alveoli (Fig. 2B).

Body weights were measured through 3 days after intratracheal administration of bleomycin in the wild-type group, untreated BLM group, and the ASC-treated BLM group, which were administered bleomycin 1 d after treatment (Fig. 2C). Untreated BLM mice showed decreased body weight (-22.7%), whereas those treated with ASCs gained weight (-13.7%) from day 2 to day 3, suggesting recovery from respiratory distress due to lung fibrosis.

To verify the therapeutic efficacy of ASC administration in more detail, hematoxylin and eosin (H&E) staining of lung sections was performed for pathological analysis. The lung tissues of all mice were removed 14 days after treatment and thin sections were stained with H&E (Fig. 2D). Interstitial areas in wild-type lungs are shown in red/purple and were very thin, whereas in lungs with pulmonary fibrosis, the interstitial areas were thicker, resulting in a wider stained area, as well as alveolar hemorrhage due to inflammation. Pathological analysis revealed that interstitial hypertrophy was markedly alleviated, and fibrosis of the lungs was reduced.

Analysis of in vivo kinetics after administration of ASCs in pulmonary fibrosis

Similar to the previous experiments, In vivo imaging systems (IVIS) Spectrum CT was performed at 10 min, 1 h, 3 h, 24 h, and 72 h after the administration of the cell suspensions for observation over time. Ten minutes after administration, fluorescence was detected in the lungs of both the wild and BLM mice, as the transplanted ASCs were physically infarcted in the lungs. However, 3 h after administration, fluorescence was observed only in the lungs of BLM-treated mice (Fig. 3A). Furthermore, at day 7 after cell administration, a similar pattern was observed (Suppl.).

Ex vivo bioanalysis after ASC administration

Mouse organs (heart, lung, liver, kidney, and spleen) were harvested 3, 6, and 24 h before and after treatment and fluorescent images were obtained using IVIS Spectrum CT (n = 3). Fluorescence decreased

over time, especially in the lungs and liver of both wild-type and BLM mice, after administration. Although no significant differences in fluorescence intensity were observed in all organs at 3 h after administration, BLM mice exhibited higher fluorescence intensity at 6 h after administration, suggesting that the transplanted ASCs remained for a relatively long time (Fig. 3B). Furthermore, BLM-mice lungs showed a greater fluorescence intensity than wild mouse lungs. Although the fluorescence intensity in the lungs significantly decreased from 3 to 6 h after administration in wild-type mice, it was not markedly decreased in BLM-mice lungs (Fig. 3C).

Localization of administered cells in lung tissue using 3D imaging analysis

Mouse lungs were harvested from BLM mice at 3, 6, and 24 h after ASC administration. The localization of these cells was observed using the tissue transparency technique Clear, UnobstructedBrain/Body Imaging Cocktails and Computational analysis (CUBIC) and 3D fluorescence imaging (Fig. 4A-C). Wild-type mice treated with ASCs were used as controls. At both 6 (Fig. 4B) and 24 h (Fig. 4C) after ASC administration, more red dots were observed in BLM-treated mouse lungs than in wild-type mouse lungs, indicating that the administered cells adhered more to the alveolar wall. ASCs were detected in a wide range of cells, not only around the bronchi, but also in the peripheral regions of the lungs. Therefore, it is possible that ASCs were transported to the fibrotic peripheral portions and became localized in the damaged lung tissue.

Discussion

Several cohort studies investigating both pirfenidone and nintedanib in IPF have reported that these drugs slow the decline in lung function, but do not increase the life expectancy of IPF patients [13]. Therefore, lung transplantation is the ultimate treatment option, but IPF remains a major challenge owing to its complexity and the limited availability of donor grafts [14].

In this study, we succeeded in establishing a technique to clarify the *in vivo* dynamics of transplanted stem cells in BLM mice based on the use of QDs, the most advanced fluorescent nanomaterial, as a label for cells. According to an official American Thoracic Society workshop report, bleomycin-induced pulmonary fibrosis has been widely used as a representative animal model of IPF that induces fibrosis in the lung tissue.

The IVIS results in this study suggested that ASCs are retained for a longer period in fibrotic lungs. In other words, this means that ASCs implanted in BLM mice accumulated slowly in the lungs and circulated in the body for a longer time compared to wild-type mice, which resulted in the suppression of fibrosis. These results suggest that ASCs transplanted into BLM mice circulate more slowly through the body and accumulate over a longer period of in the lungs than in wild-type mice, thereby reducing fibrosis. This suggests that ASCs administration had a therapeutic effect on fibrosis recovery. QDs are hydrophobic and fabricated with toxic heavy metals, such as Cd and Se; there are limited reports

regarding their actual application in bioimaging. However, water-soluble and low-toxicity QDs have been created recently via coating them with molecular polymers and the modification of polar molecules on the surface to form a shell layer. These developments have greatly advanced the possibilities for application in biotechnology and have promoted the development of associated cell imaging, medical diagnostics, and pharmacokinetic monitoring [2–5].

This study demonstrates that the highly sensitive imaging of ASCs behavior after transplantation, which was previously unexplored, is possible without organ removal. Furthermore, this imaging technique demonstrated that ASCs were deposited in significant numbers over the entire lung area in a mouse model of pulmonary fibrosis, thereby providing a therapeutic effect. ASCs contain many growth factors, such as vascular endothelial growth factor, hepatocyte growth factor, MMP-2 (Matrix Metalloproteinase-2), TSG-6 (Tumor necrosis factor-stimulated gene-6), and IL-10(Interleukin-10) [23]. Specifically, MMPs are known to be factors that suppress fibrosis. In addition, since TSG-6 and IL-10 are immune regulatory genes, we speculate that these genes may play an inhibitory role against fibrosis caused by overactive immune responses via the induction of pro-inflammatory cytokines [18–22].

The application of QDs to accurately monitor the *in vivo* kinetics of transplanted cells raises expectations for *in vivo* diagnosis and treatment in clinical applications [15]. As reported here, QDs can be used to detect dynamic changes in transplanted cells and have potential future applications in preclinical studies in infectious diseases, malignant tumors, autoimmune diseases, immunodeficiency diseases, and transplantation medicine. Additionally, QD applications are expected to be developed for regenerative medicine in the future [16]. The primary bottleneck in clinical applications is the long-term safety of the organisms, which requires detailed studies on long-term toxicity and dosage. Further development and research are expected.

In summary, this study reports a technique for labeling stem cells with QDs and the imaging of labeled cells *in vivo*, successfully demonstrating the efficacy of stem cell therapy in a model of pulmonary fibrosis. The QDs did not affect the viability or proliferation of ASCs and the *in vivo* dynamics demonstrated that tissue transparency and 3D fluorescence imaging using the CUBIC method can be integrated for comprehensive imaging. However, there are still many unanswered questions in this field [17]. The applications of QDs with stem cells are just beginning to be explored. Stem cell therapy in lung regenerative medicine is still in its early stages and many challenges remain to be explored, such as immune rejection and the possibility of tumor formation. Therefore, synergistic interdisciplinary studies in the fields of biology, chemistry, and engineering are required. The development of advanced imaging modalities and tools is expected to be a breakthrough in nanotechnology and regenerative medicine.

Methods

Animal ethics approval

Six-week-old female C57BL/6JJmsSlc mice were purchased from Japan SLC, Inc. (Shizuoka, Japan). All mice were housed at Nagoya University under a constant temperature (21–23°C) and a 14-hour light, 10-hour dark cycle and provided food and water ad libitum. All procedures involving mouse experiments were approved by the Committee on Animal Experiments of Nagoya University (M230269-003) and performed in accordance with the institutional and national guidelines. The reporting of animal experiments adheres to the ARRIVE guidelines (https://arriveguidelines.org/arrive-guidelines).

Bleomycin-induced pulmonary fibrosis model

Female 6-week-old C57BL/6JJmsSlc mice (Shizuoka, Japan) were anesthetized with a combination anesthetic cocktail (0.3 mg/kg body weight of medetomidine, 4 mg/kg body weight of midazolam, and 5 mg/kg body weight of butorphanol) by intraperitoneal injection and then received a single endotracheal dose of 100 μg of bleomycin (Nippon Kayaku Co., Ltd., Japan) on day 0 to induce pulmonary fibrosis. Control animals received phosphate-buffered saline (PBS) via the same route.

ASC isolation and culture

MSCs and lung fibroblasts were obtained from mice. Fresh inguinal fat was isolated from mice by using Dulbecco's PBS (Gibco, Billings, MT, USA). Adipose tissue was cut into small pieces and then digested with 2mg/mL of type I collagenase (Sigma-Aldrich, St. Louis, MO, USA) for 60 min at 37°C on a shaker. Cells were resuspended after centrifugation at 1,500 rpm for 5 min and then filtered through a 0.22 μm filter mesh (SLGV033RS, Millex-GV; Merck Millipore Ltd., Burlington, MA, USA) to remove any tissue residue. After washing twice, cells were resuspended in DMEM/F12 (11965-092; Gibco, Billings, MT, USA) containing 10% fetal bovine serum (Gibco, Billings, MT, USA) and seeded in T75 tissue culture flasks (BD, Franklin Lakes, NJ, USA). Cells were cultured in a humidified 5% CO_2 incubator at 37°C. The floating cells were removed after 24 h and the media was changed after 3 days. At 90% confluence, cells were detached using 0.25% trypsin-EDTA and passaged.

ASC transplantation

ASCs were cultured until they reached confluence and then 2×10 cells were placed in 8 nM QD-R8 (Qdot 800 ITK(TM) carboxyl quantum dots, Q21371MP; Invitrogen, Waltham, MA, USA) solution at 37°C and 5% CO_2 for 24 h. ASCs were then collected and resuspended in PBS: 135 μL of PBS and 15 μL of heparin were used for every 1 × 10^6 ASCs. On day 7 after fibrosis induction, the treated group received a single intravenous (tail vein) dose of ASCs (150 μL; 5 × 10^6 ASCs).

IVIS Fluorescent Imaging

In vivo fluorescence imaging of ASCs labeled with QDs was performed using an IVIS Spectrum CT (PerkinElmer, USA) at 10 min, 1 h, 3 h, 24 h, 48 h, and 72 h after tail vein administration. During image acquisition, the mice were anesthetized with isoflurane. The imaging parameters were as follows: excitation wavelength, 745 nm; fluorescence wavelength, 800 nm; and exposure time, 5 s. The heart, lung, liver, kidney, and spleen were excised 3, 6, and 24 h after cell administration to evaluate the *in vivo*

dynamics of each organ and images were captured using an IVIS Spectrum CT. Images were analyzed, and the accumulation efficiency was calculated based on the drawn region of interest (ROI).

X-ray CT analysis

A Latheta LCT-200 X-ray CT scanner for laboratory animals was used for CT analysis. All mice were anesthetized with isoflurane during imaging and placed in a 48 mm fixture for the field of view. The imaging conditions are presented in Table 1. CT imaging of ASCs labeled with QDs was performed using an IVIS Spectrum CT (PerkinElmer, USA) on days 1, 3, 7, and 14 after tail vein administration. Images were analyzed and lung volume was calculated based on the drawn ROI. The range of CT values was set at -900 to -200 so that bone and fat were not measured.

Table 1
X-ray CT imaging conditions

Radiographic Condition	Setting Value
Field of view	48 mm / 80 mm
Pixel size (μm)	48 / 80
Slice thickness (μm)	192 / 320
Slice interval (μm)	192 / 320
Rotation speed	4 x
Rotation angle (°)	360
X-ray tube voltage	Low
Number of projection directions	1,592
Artifacts removal target	soft-tissue, lung
Metal artifact elimination	No
Video synchronization	respiratory gating

Measurement of surfactant protein D concentration

The trachea of the mouse on days 3 and 5 after isoflurane administration was exposed, the upper tracheal surface was split, a sonde was inserted, and the trachea was ligated. A total of 500 μL of PBS was administered into the trachea via the sonde. When it had been distributed to the lung, it was backflushed and then collected into a 1.5 mm tube. This procedure was repeated three times, for a total of 1,500 μL of PBS collected after washing the lungs. This collected alveolar lavage fluid was − 80℃ frozen immediately.

The SP-D concentration in the alveolar lavage fluid was measured using a Quantikine Mouse SP-D ELISA kit (Biotechne, Minneapolis, MN, USA).

CUBIC tissue clearing

The CUBIC-L solution for delipidation and decolorization was prepared as a mixture of 10%/10% (wt/wt) Triton X-100 (Sigma-Aldrich, St. Louis, MO, USA)/N-butyldiethanolamine (B0725; Tokyo Chemical Industry, Tokyo, Japan). The CUBIC-R solution was prepared as a mixture of 30% (w/v) nicotinamide (Sigma-Aldrich, St. Louis, MO, USA) and 45% (w/v) antipyrine (Sigma-Aldrich, St. Louis, MO, USA).

For whole-organ clearing, 4% PFA fixed lungs were washed three times with PBS and then immersed in CUBIC-L solution (50% (v/v) mixed with water) for 6 h at 37°C. The organs were then immersed in CUBIC-L solution at 37°C for 48 h; the solution was refreshed at 24 h during this process. After decolorization and lipid clearing, the organs were washed with PBS at room temperature (or 21–23℃) for 2 h, followed by immersion in the CUBIC-R solution (50% (v/v) mixed with water) for 6 h at room temperature. Finally, the organs were immersed and stored overnight in the CUBIC-R solution at room temperature. After clearing the tissue, measurements were performed using a light sheet microscope (UltraMicroscope II; Miltenyi Biotec, Bergisch-Gladbach, Germany).

Declarations

Data Availability

The datasets used and/or analysed during the current study available from the corresponding author on reasonable request.

Acknowledgements

The authors thank Dr. Kazuhide Sato for providing comments and gratefully acknowledge the technical support provided by Yoshimi Kato and Yushi Nishimura. The authors wish to acknowledge the Division for Medical Research Engineering, Nagoya University Graduate School of Medicine, for the use of CM 3050 S and BZ-9000.

Funding

This study was supported by Grants-in-Aid for Scientific Research from the Japan Society for the Promotion of Science (grant numbers 22H03938 and 21H05589) and the Advanced Research Infrastructure for Materials and Nanotechnology in Japan (ARIM, Nagoya University) of MEXT.

Author Contributions

Conception and design of the work: N.H. and H.Y. Acquisition and analysis: S.M., Y.B., and H.Y. Interpretation of data: S.M. and S.S. Writing the original draft: M.M. and S.M. Review and editing: M.M. and H.Y. All authors approved the final version of the manuscript.

References

1. Martinez, F. J. *et al.* Idiopathic pulmonary fibrosis. *Nat. Rev. Dis. Primers* **3**, 17074 (2017).
2. Natsuizaka, M. *et al.* Epidemiologic survey of Japanese patients with idiopathic pulmonary fibrosis and investigation of ethnic differences. *Am. J. Respir. Crit. Care Med.* **190**, 773–779 (2014).
3. John, A. E., Joseph, C., Jenkins, G. & Tatler, A. L. COVID-19 and pulmonary fibrosis: A potential role for lung epithelial cells and fibroblasts. *Immunol. Rev.* **302**, 228–240 (2021).
4. Montes Ruiz Cabello, M., Callejas Rubio, J. L. & García Villanova, P. Fibrosis pulmonar idiopática y determinaciones serológicas de autoinmunidad. *Med. Clin. (Barc)* **160**, 181 (2023).
5. Ley, B., Collard, H. R. & King, T. E. Clinical course and prediction of survival in idiopathic pulmonary fibrosis. *Am. J. Respir. Crit. Care Med.* **183**, 431–440 (2011).
6. Koudstaal, T. & Wijsenbeek, M. S. Idiopathic pulmonary fibrosis. *Presse Med.* **52**, 104166 (2023.
7. Serrano-Mollar, A. Cell therapy in idiopathic pulmonary fibrosis†. *Med. Sci. (Basel)* **6**, 64 (2018).
8. Chan, W. C. *et al.* Luminescent quantum dots for multiplexed biological detection and imaging. *Curr. Opin. Biotechnol.* **13**, 40–46 (2002).
9. Dahan, M. *et al.* Diffusion dynamics of glycine receptors revealed by single-quantum dot tracking. *Science* **302**, 442–445 (2003).
10. Larson, D. R. *et al.* Water-soluble quantum dots for multiphoton fluorescence imaging in vivo. *Science* **300**, 1434–1436 (2003).
11. Ogihara, Y. *et al.* Labeling and in vivo visualization of transplanted adipose tissue-derived stem cells with safe cadmium-free aqueous ZnS coating of ZnS-AgInS2 nanoparticles. *Sci. Rep.* **7**, 40047 (2017).
12. Shipley, J. M., Wesselschmidt, R. L., Kobayashi, D. K., Ley, T. J. & Shapiro, S. D. Metalloelastase is required for macrophage-mediated proteolysis and matrix invasion in mice. *Proc. Natl Acad. Sci. U. S. A.* **93**, 3942–3946 (1996).
13. Francesco, A. *et al.* Efficacy of Pirfenidone and Nintedanib in Interstitial Lung Diseases Other than Idiopathic Pulmonary Fibrosis: A Systematic Review. *Int J Mol Sci.* **24**, 7849. (2023)
14. Cottin, V. *et al.* Fibrosing interstitial lung diseases: knowns and unknowns. *Eur. Respir. Rev.* **28**, 180100. (2019).
15. Hiroshi, Y., *et al.* Theranostics applications of quantum dots in regenerative medicine, cancer medicine, and infectious diseases. *Adv. Drug. Deliv. Rev.* **200***, 114863-114863.* (2023).
16. Shota, Y., *et al.* In Vivo Real-Time Quantum Dots Imaging to Track Transplanted Adipose Stem Cells in Different Inflammatory States of Acute Liver Failure Mice. *Cell Transplant.* **32**:9636897231176442. (2023).
17. Ma, S. *et al.* Current Status of Stem Cells and Regenerative Medicine in Lung Biology and Diseases. *Stem Cells.* **32**, 16–25 (2014).
18. Daniel J. Weiss., Immunobiology of mesenchymal stem cells. *Cell Death Differ.* **21**, 216–225 (2014).
19. Giannandrea, M. & Parks, W. C. Diverse functions of matrix metalloproteinases during fibrosis. *Dis. Model. Mech.* **7**, 193–203 (2014).

20. Ren, G. *et al.* Species variation in the mechanisms of mesenchymal stem cell-mediated immunosuppression. *Stem Cells* **27**, 1954–1962 (2009).
21. Choi, H., Lee, R. H., Bazhanov, N., Oh, J. Y. & Prockop, D. J. Anti-inflammatory protein TSG-6 secreted by activated MSCs attenuates zymosan-induced mouse peritonitis by decreasing TLR2/NF-κB signaling in resident macrophages. *Blood* **118**, 330–338 (2011).
22. Sreeramkumar, V., Fresno, M. & Cuesta, N. Prostaglandin E2 and T cells: friends or foes? *Immunol. Cell Biol.* **90**, 579–586 (2012).
23. Fukase, M. *et al.* Intravenous injection of human multilineage-differentiating stress-enduring cells alleviates mouse severe acute pancreatitis without immunosuppressants. *Surg. Today* **52**, 603–615 (2022).

Figures

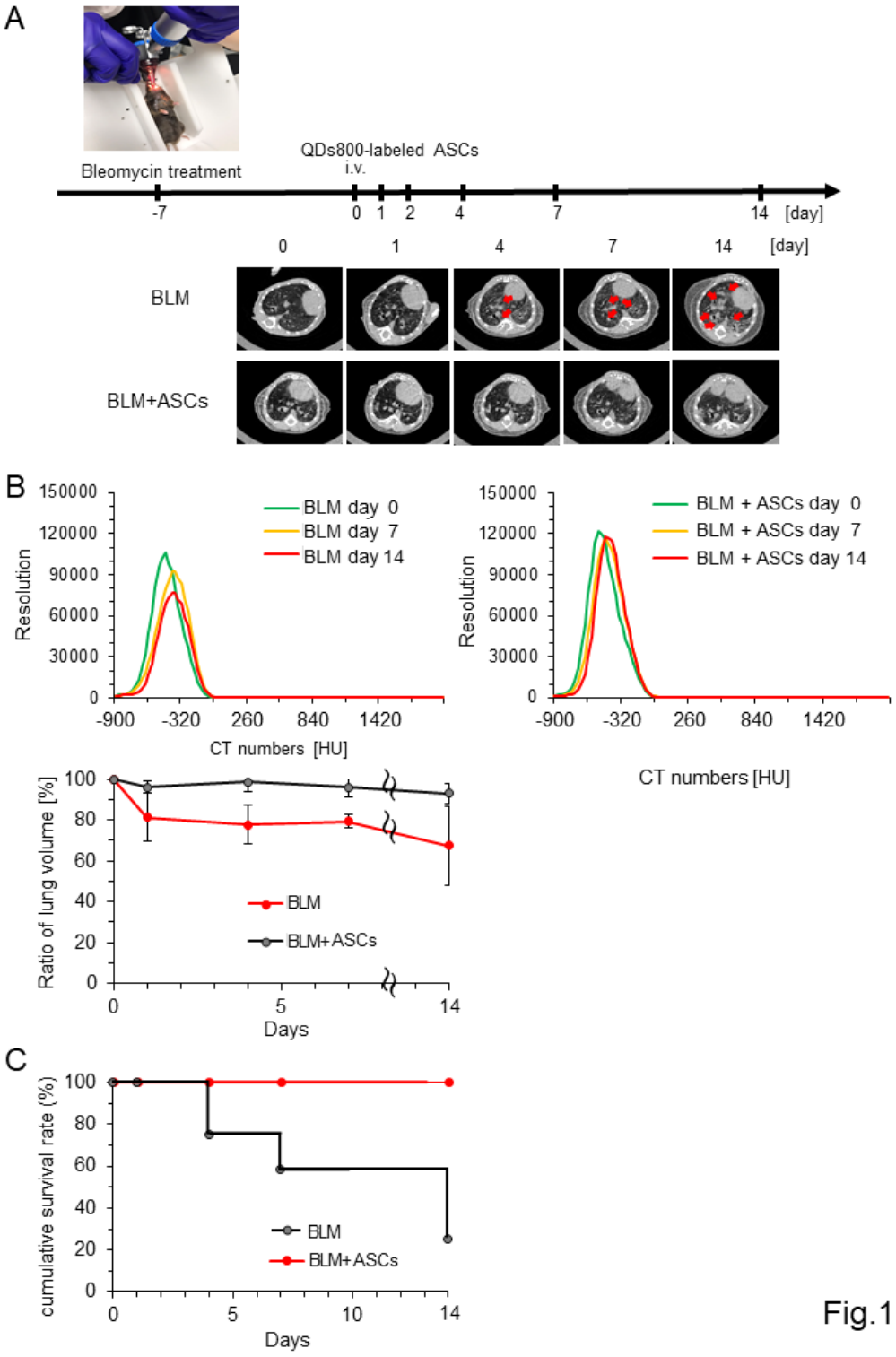

Figure 1

Effects of ASCs administration at different post-injection times using CT analysis.

(A) Time course of bleomycin and ASCs administration and cross-sectional lung images using CT analysis. Red arrow, fiberization; (B) (upper panel) Histogram of CT values. Green line, days after ASCs or PBS administration on BLM-mice (lower panel) changes in lung volume with time. Red line treated control

of BLM-mice; Black line, ASCs treatment; (C) cumulative survival rate. Red line, treated control of BLM-mice; Black line, ASCs treatment.

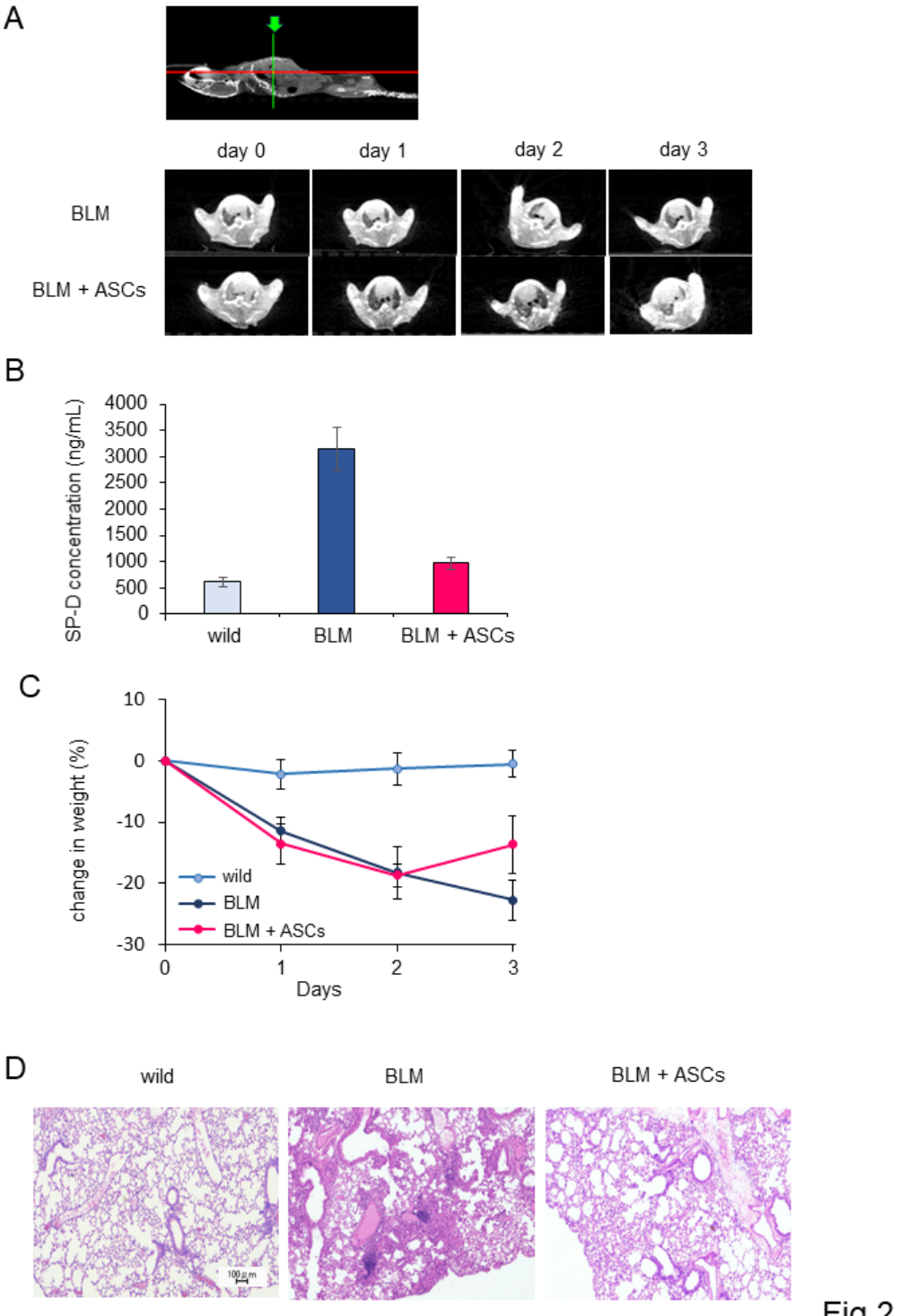

Fig.2

Figure 2

ASC Therapeutic Effects on Fibrosis Suppression.

Micro-CT imaging during bleomycin-induced lung fibrosis. (A) 3D Micro-CT imaging at green line of progressive pulmonary fibrosis in a representative saline and bleomycin-treated mouse over time. Mice were scanned daily, from baseline to 3 days after induction. (B) Surfactant protein levels in bronchoalveolar lavage fluid (BALF) levels at day3 after ASCs injection evaluated by ELISA. (C) Body weight loss in bleomycin treated mouse. The body weight on day 0 was defined as 100%. The relative body weight was calculated as a percentage of that measured on day 0. (D) Fibrotic histopathologic changes in the tissue were observed via H&E staining.

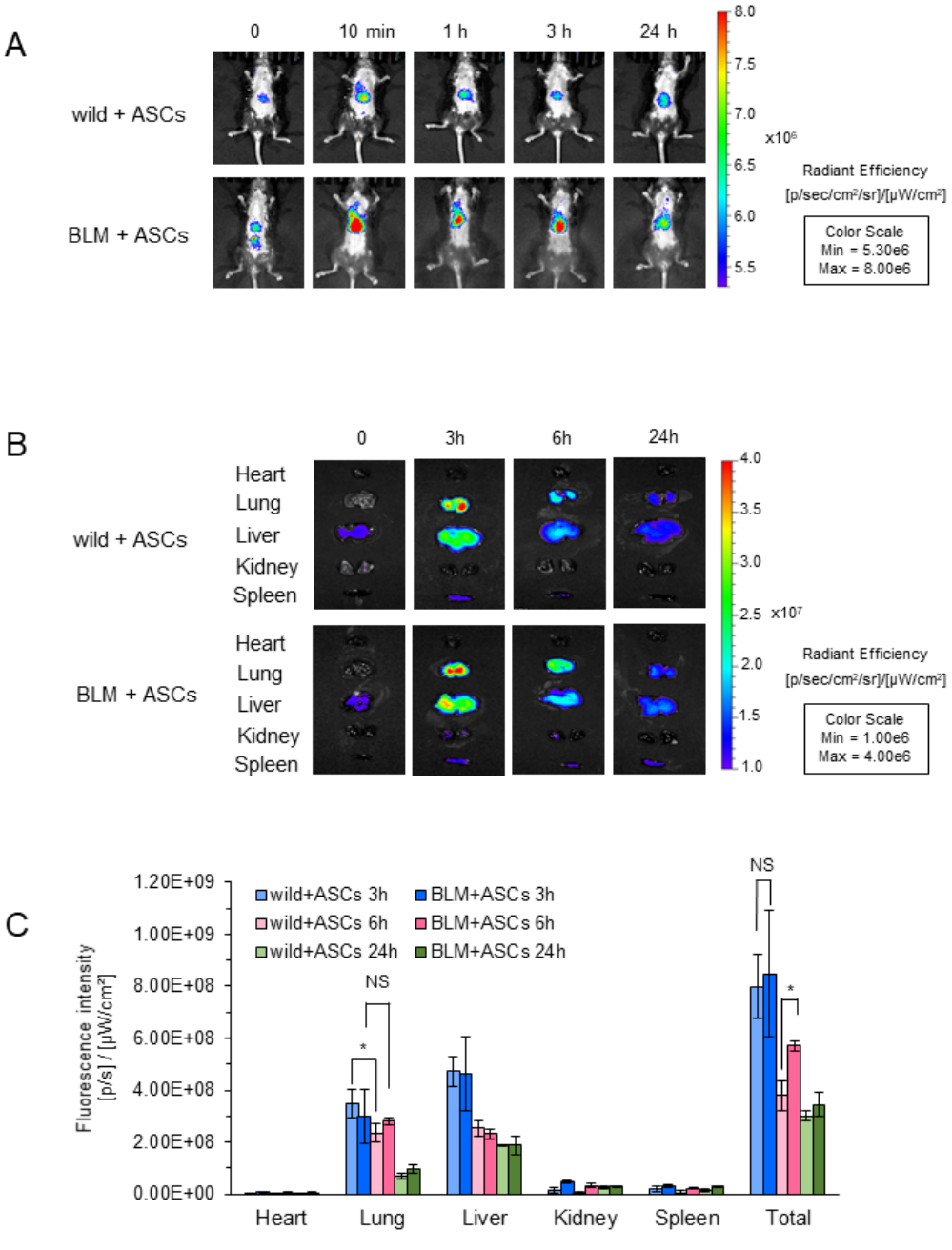

Fig.3

Figure 3

Whole body distribution of QDs800-labeled ASCs following IV at different time points.

(A) Representative wildtype or BLM-mice transplanted with ASCs. (B) Fluorescent images of normal tissues and BLM-mice excised from the mice treated with different samples at 3, 6, and 24 h after injection. (C) Quantitative analysis of tissue distribution of QDs at 3, 6, and 24 h after ACSs injection.

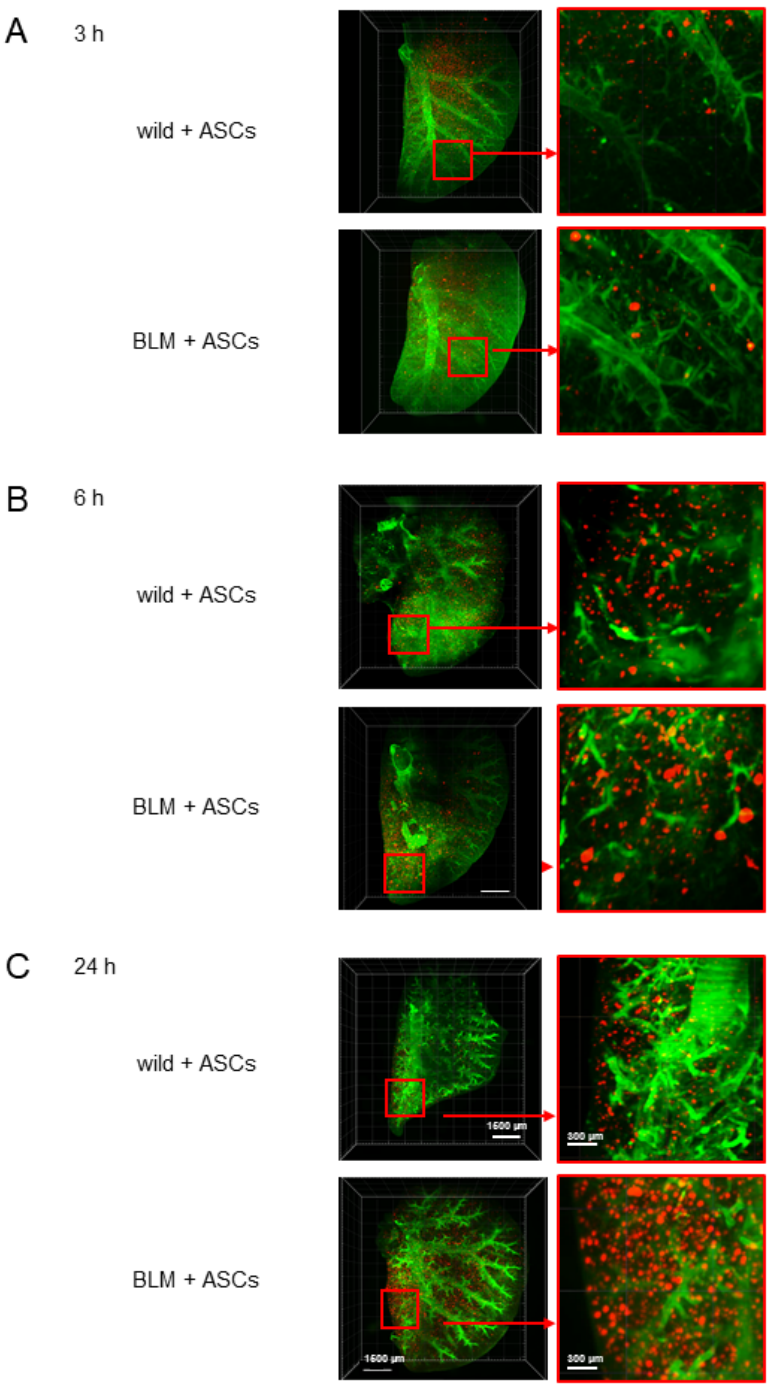

Fig.4

Figure 4

Distribution of QDs800-labeled ASCs in whole mouse lung

Maximal projections of light sheet acquisitions from whole mouse lungs sampled at 3, 6, and 24 h after ACSs injection. The lung was subjected to whole-organ clearing protocol and immunostained with Alexa 488-conjugated anti-α-SMA antibody (green) and QDs800-labeled ASCs (red). (A) 3h after ACSs injection. (B) 6 h. (C) 24 h.

Supplementary Files

This is a list of supplementary files associated with this preprint. Click to download.

- Suppl.2BLMASCs.mp4
- Suppl.2wildASCs.mp4
- supplementaryfigures.pptx